EWGAE 33rd European Conference on Acoustic Emission Testing
12-14 September 2018 - Senlis - France

COMBINATION OF SYNCHROTRON COMPUTED TOMOGRAPHY AND ACOUSTIC EMISSION MEASUREMENTS FOR CYCLIC LOADING OF FIBRE-REINFORCED COMPOSITES

Philipp Potstada[1], Sebastian Rosini[2], Mark Mavrogordato[2], Ian Sinclair[2], S. Mark Spearing[2], Markus G. R. Sause[1]

[1] University of Augsburg, Institute for Materials Resource Management, Mechanical Engineering, D-86135 Augsburg
[2] University of Southampton, Faculty of Engineering and the Environment,

Abstract:

During incremental load-unload cycles of fibre-reinforced materials, the re-initiation of acoustic emission below the previously reached load is frequently observed. This is known as the Felicity effect and its physical origin has been discussed in the community for several decades. The principal explanations for this effect are the rubbing together of existing crack faces which thus act as tribological acoustic emission sources or the initiation of new damage because of material stress-relaxation during the unloading phase. We conducted combined acoustic emission measurements and high-resolution synchrotron computed tomography experiments on a carbon fibre / epoxy prepreg system. Samples were prepared as double-edge notched tensile specimens with [±45 0 ±45], [0 90_3 0] and [90 0_3 90] layups. At a voxel resolution of 1.625µm, we were able to visualize the growth of damage as a function of applied load/unload steps in a sequence of volume images. With the simultaneously acquired acoustic emission signals, this allows identification of the origin of the source volumetrically, as three volumes were taken per load step in situ. These investigations are part of an ongoing measurement campaign and represent a first interpretation towards the physical origin of the early acoustic emission onset in fibre-reinforced materials. This provides a first step to reveal the origin of the Felicity effect in fibre-reinforced materials.

1. Introduction

Fibre-reinforced polymer composites are used in transport applications because of their strength/weight and stiffness/weight ratios to reduce component weight, and hence to provide greater fuel efficiency and lower emissions. However, predicting damage formation and progression remains challenging, so conservative design levels are used and safety-relevant components need to be re-qualified frequently.

Acoustic emission (AE) sensing represents a core non-destructive testing technology for composite materials in transport applications, in which transient elastic waves, linked to sudden stress redistribution phenomena (such as micro-cracking, interface sliding) are used to detect and quantify damage processes. In many safety-critical applications of fibre-reinforced polymers such as pressure vessels, aerospace structures and similar, qualification and re-qualification of components makes use of the measurement of the so-called Felicity ratios (FR) as introduced by Timothy Fowler [1].

In his pioneering work, Joseph Kaiser demonstrated for metallic materials, that AE usually starts after exceeding the previous load level [2]. However, as first pointed out by Timothy Fowler, in fibre-reinforced polymers, the AE signals usually initiate at lower load levels than

those previously achieved [1]. After almost 40 years of scientific debate [3]–[10], no convincing experimental evidence has hitherto been provided that clearly explains the source of such early AE signals in FRPs and thus explains why these materials apparently violate the Kaiser effect [1].

In the scientific community there are essentially two principal ways of interpreting this early onset of AE:

1. Microscopic relaxation, viscoelastic behaviour and "settling" of the material cause local stress levels, that are sufficient to initiate new damage at macroscopic load levels, lower than those previously reached;

2. Stick-slip friction (rubbing) of existing crack walls causes AE, which is not related to any microscopic or macroscopic damage formation.

As stick-slip friction is a well-known source of AE, it cannot be excluded, that all or part of the early AE originates from this source. Revealing that such non-damage related AE acts as an indicator for the structural integrity of a fibre-reinforced polymer would immediately question the validity of current testing routines, as accept / reject decisions are then taken based on friction signals, not damage growth. In addition, the formation of new microscopic damage as consequence of local stress redistribution is another aspect, which is rarely taken into account in structural analysis and definition of test procedures.

Previous work using synchrotron radiation computed tomography (SRCT) has demonstrated that damage mechanisms, such as individual fibre fractures, matrix cracking, and other damage mechanisms can be reliably located and quantified [11], [12]. Thus, with the ability to observe visually the initiation and growth of new damage at low load levels and to distinguish this versus the relative movement of crack walls due to stick-slip friction we expect to make a key contribution to this scientific and engineering question.

This paper presents initial data demonstrating that it is possible to acquire AE-signals during an in situ SRCT loading experiment at the European Synchrotron Radiation Facility (ESRF) in Grenoble France. In this study, we present first results to correlate the AE signals recorded during load/unload cycles of a carbon/epoxy material with the occurrence of microscopic damage identified by SRCT.

2. Experimental

For the experiments at the ESRF, the microtomography beamline ID19 was chosen in order to provide optimal image fidelity at the resolution required. For the in situ acquisition, a combination of a MISTRAS PCI-2 AE-system and a modified DEBEN CT5000 tensile stage proven in previous studies was used [13], [14]. The AE measurement chain consists of a miniature multi-resonant sensor HD2WD from MISTRAS. Two AE sensors were used to allow a one-dimensional AE source localization. The acquired signals were amplified by a MISTRAS 2/4/6 pre-amplifier and were subject to a built-in analogue 20-1200 kHz band-pass-filter. Preamplifiers were mounted on the rotation table close to the in situ tensile load stage. The amplified AE signal was led outside the experimental hutch using a standard RG58 coaxial cable, which connects to the PCI-2 acquisition card. The acquired signals were recorded with the MISTRAS software AEwin^{TM}.
The load was applied by a commercial CT5000 DEBEN^{TM} U.K. in situ tensile stage connected via the associated controller box to a standard PC using software provided by DEBEN^{TM} U.K.

While the drive unit and the load cell of the tensile stage remained unmodified relative to the commercial setting, the load introduction concept of the specimen was modified (see Figure 1).

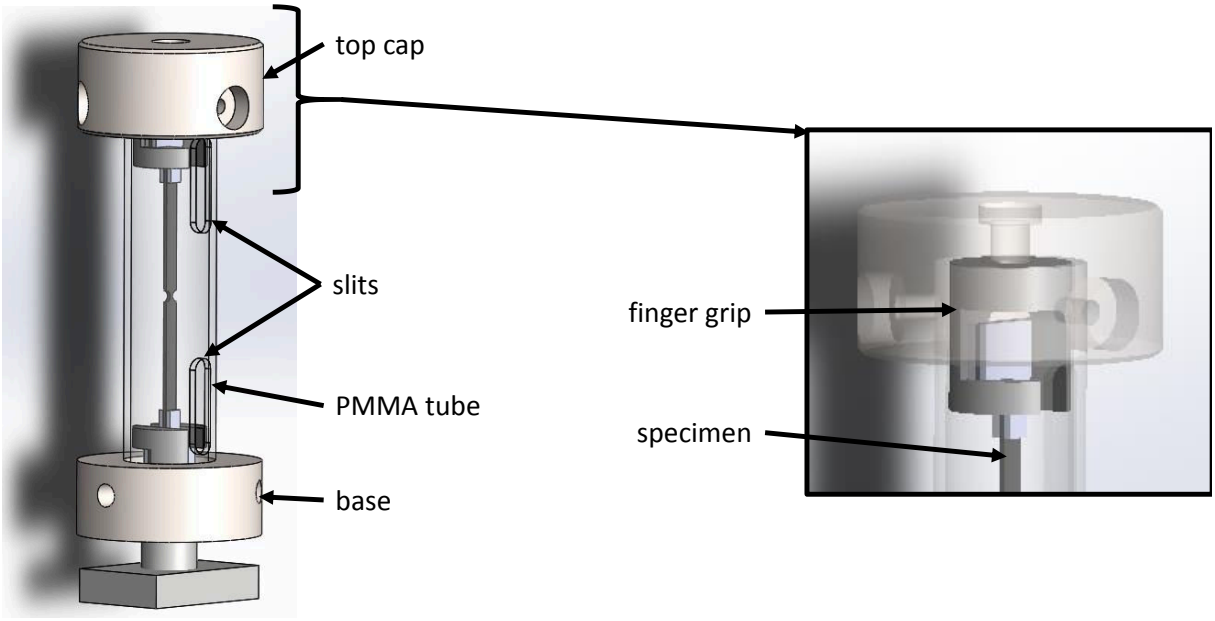

Figure 1. Modified part of the in situ tensile stage with finger grip clamping system and PMMA tube with two inserts for acoustic emission sensors cables.

The load was introduced via a finger grip system, which ensures a simple assembly of the specimen and a proper load transfer into the specimen after reaching a slight pre-load. The upper finger grip was statically fixed in a top-cap, which transferred the load via a PMMA tube into a custom-made frame of the tensile stage. To ease assembly of the PMMA tube, it was held in position with three screws. For synchronous evaluation of mechanical load and acoustic emission data, the current force values were fed into the AE system by a proportional analogue voltage signal.

Based on the explanations in Section 1, to reveal the origin of the Felicity effect, it is necessary to induce step-wise crack growth and potential friction effects during load-unload experiments. Accordingly, we used three different multi-angle layups, which allow growth of a crack network before ultimate failure of the specimen. In addition, based on the layup we also expect a certain likelihood of mutual crack interaction and the occurrence of crack surface friction. Based on earlier investigations by Wright et al. [15], we prepared double edge notched tensile specimens via waterjet cutting from [±45 0 ±45], [0 90_3 0] and [90 0_3 90] laminate plates. All laminates were produced from carbon/epoxy prepreg, Sigrafil™ CE1250-230-39 following the material supplier's specifications. T-shaped aluminium tabs were adhesively bonded to the specimen specimen ends. A grinding and cleaning phase on the contact surface between tabs and coupons took place before application of fast curing methyl-methacrylate adhesive. To ensure adhesion and mechanical stability of the AE sensors on the specimens, holders were fabricated out of polylactide by additive manufacturing and attached tightly to the specimens using rubber rings. To obtain a repeatable and correct positioning of the support structure, the holders include four integrated dowel pins (as indicated in Figure 2).

At the beginning of each test, three pencil lead breaks (PLB) were performed at the base of the tensile stage to ensure a sufficient coupling of the AE-sensors to the specimen. The setting used for the AE-acquisition for both sensors were a threshold of 35dB$_{AE}$ at 40dB$_{AE}$ pre-amplification and a Peak Definition Time (PDT) of 10µs, a Hit Definition Time (HDT) of 80µs and a Hit Lockout Time (HLT) of 300µs. The AE signals were acquired with a sampling rate of 10 MS/s.
After a satisfactory pre-check, the AE-acquisition was started. A first SRCT scan was collected to record the initial (undamaged) specimen volume. To ensure a proper alignment of the specimen in the beam path, a load of 15 N (representing a small percentage of the sample ultimate tensile strength) was applied. At this load level, no pre-damage was observed. The drive unit was switched off and the cross-head position was kept constant by the self-locking mechanics of the loading stage. The scan was performed continuously with beam energy of 19.5 keV. During each tomographic scan, 2996 projections with an exposure time of 50 ms were collected at a detector distance of 50 mm. The voxel size was 0.65 µm.

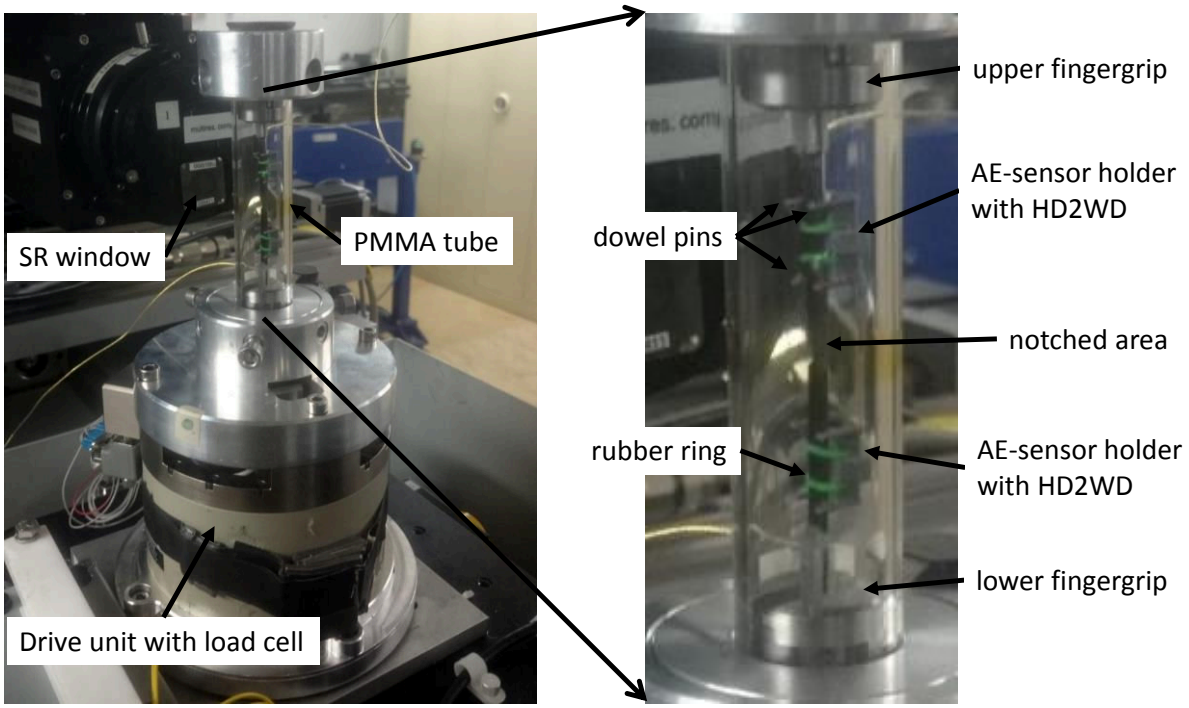

Figure 2. In situ tensile stage with installed specimen and AE sensors ready for testing.

For the evaluation of the Felicity effect, load/unload experiments are carried out at a constant displacement rate of 0.2 mm/min. Typically, the load is increased to some nominal target value L_1, then reduced and increase again to a higher value L_2. This is continued for increasing loads until the material fails at a value L_{max}. At the first occurrence of significant acoustic emission during the reload cycle, the load level B_2 is defined. This allows calculation of the Felicity ratio FR for the second load cycle according to $FR = B_2/L_1$. In order to reveal the origin of the Felicity effect, we follow a slightly modified load schedule in this investigation. Other than pre-defined step-wise increased loading, test were interrupted after the occurrence of a sequence of acoustic emission signals (e.g. > 5 signals). After reaching this peak load, the specimens are unloaded by 10% of the peak load. Two more load/unload cycles are carried out with the same peak load as seen in the examples of Figures 6-8.This allows the virgin Felicity ratio to be determined at each load level and to distinguish this from subsequent loading to the same

load level. At each plateau phase seen in Figures 6-8, additional SR scans are taken to assess the occurrence of damage progression. Two more peak load increments are carried out for each sample to induce a certain amount of damage progression. For the three different sample types, the ultimate tensile strength was calculated as 577 MPa for [±45 0 ±45], 736 MPa for [0 90_3 0] and 1046 MPa for [90 0_3 90] layups.

2.1. Acoustic emission evaluation

For the acquired AE signals, a feature extraction routine was performed. Besides the common AE feature values of amplitude, energy, duration, also the partial powers of six equal frequency ranges of 150 kHz width, ranging from 0 MHz to 1 MHz were calculated out of the first 35 µs after the arrival time. The arrival time was calculated using the Akaike information criterion (AIC) [16]. In addition, spectral feature values, such as the weighted peak frequency and frequency centroid were calculated from FFT spectra of the signals (see [17] for precise definition of features). A first data reduction was carried out to remove erroneous AE signals resulting from driver motor control signals. These were easily identified based on their unique frequency characteristics and their time of occurrence of the direction of load reversal.

Furthermore, AE sources were localized using a classical Δt-based algorithm considering the given geometry of the specimen and the sensor positions. The velocity of sound was measured for each material using time-of-flight tests on the raw material plates before cutting the test geometries. Only the AE-signals localized within 50±3 mm around the notch centre were used for the following evaluation. This limitation is necessary to conform with the observation volume of the SR scans, i.e. to reach an equivalent data basis for both methods.

A pattern recognition approach following [18] was performed using a Gustafson-Kessel algorithm allowing a maximum number of $P = 6$ clusters and a minimum number of $M = 4$ features for 12 previously selected list of frequency features K. The selected features are reverberation frequency, average frequency, initiation frequency, partial power 1-6, peak frequency, frequency centroid and weighted peak frequency. Similar to other specimens tested in this experimental setting [19], two clusters are identified in this optimization procedure. Based on conclusions of earlier investigations [17], [20], [21] and direct validation within [19], these are ascribed to the occurrence of fibre breakage (high frequency cluster) and to the occurrence of matrix cracking and interfacial related mechanisms (low frequency cluster).

For the evaluation of the Felicity ratio, a modified procedure originally published in [4], [22] was proposed to stabilize the numerical values [23]. In contrast to this, for this investigation, we use the most conservative approach and take the load level of the first acoustic emission signal as the onset value for the definition of the Felicity ratio. Additionally, we distinguish between signals of both clusters, e.g. we calculate separate Felicity ratios for fibre breakage and matrix cracking / interfacial failure related AE signals.

2.2. SRCT evaluation

Ten scans of the same region of interest (showed in Figure 4) were collected, while the specimens were increasingly loaded (and strains increased). To ensure at a micro-metre scale that the same region could be investigated while damage progressed, a registration of the scanned volumes was made by visual inspection. The user was asked to recognise a unique feature (e.g. a particular pattern in the top view of the fibres) and to record the position of this feature in all the scanned volumes. Based on this, all the volumes were cropped and aligned to a same position along the specimen length. All the scans were loaded onto the software

VGStudio MAX™ and the volume recorded at the highest strains was observed first. Cracks were visually detected and segmented using a growth segmentation tool available within the software. The user was able to identify the most developed cracks and reduce the time needed to investigate the volumes at lower strains as the centroids of the segmented cracks had approximately the same coordinates in all the registered volumes. By visual check and use of the automated growth segmentation tool it was then possible to record the evolution of a particular crack. An example of a crack detected with the automated tool is shown in Figure 3 were both the contours of the less and more developed crack are shown respectively in dark and lighter cyan.

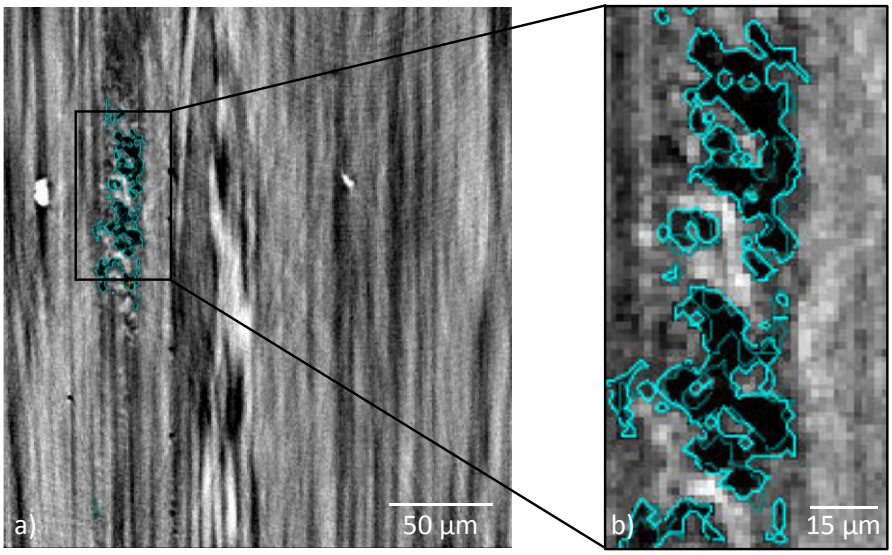

Figure 3. a) Crack evolution as identified on a single slice of the highest strains scanned volume b) zoomed region showing in black the crack at the highest strains with its contours in light cyan. In darker cyan, the contours of the same less developed crack as detected with the growth segmentation tool in a scanned volume at lower strains.

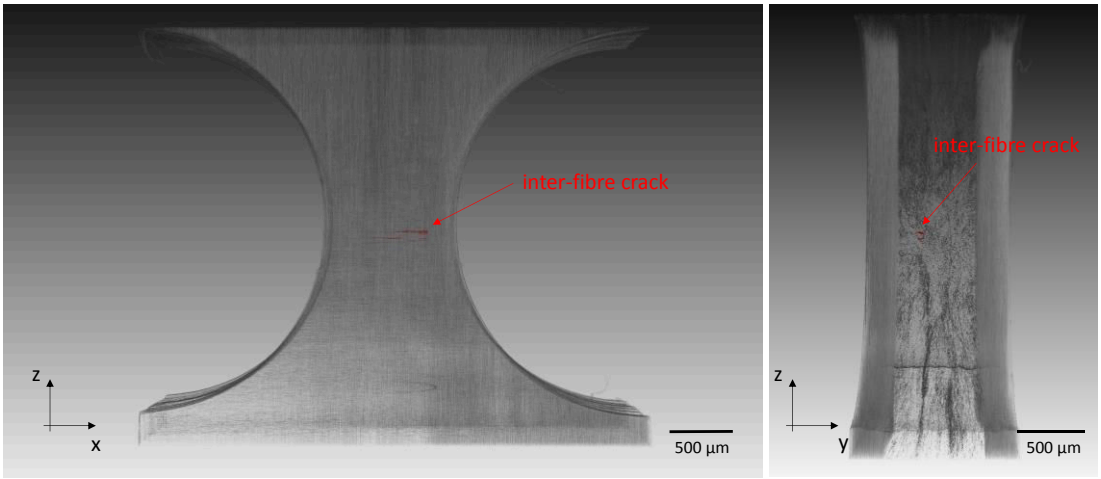

Figure 4. Frontal (left) and lateral (right) view of the region of interest, kept the same for all the scanned volumes. The inter-fibre crack is shown in red as identified in the highest strains scans. The combined use of a visual approach and an automated growth segmentation tool on VGStudio MAX™ allowed the user to identify the crack evolution from lower to higher strains.

3. Results

In the following, the results of the in situ investigations are presented, using combined AE and SRCT measurements, distinguished based on the stacking sequence used.

3.1. Layup [0 90_3 0]

As the first case, a cross-ply stacking with a predominantly 90° fibre orientation relative to the load axis is studied. With increasing load, the occurrence of transverse matrix cracks (inter-fibre cracks) is observed, see Figure 5. In addition, fibre breakage is observed to occur in the 0° plies. From SRCT observations, no growth of delamination between the 0° and 90° plies was observed. Figure 6 shows the acoustic emission results of one specimen. Based on the pattern recognition results, cumulative hits for both signal classes are superimposed on the load-time curves. Each cycle with occurrence of acoustic emission additionally holds the corresponding Felicity ratios for each signal class. For this cross-ply stacking, all Felicity ratios were > 0.99, rendering it impossible to discuss the origin of acoustic emission signals at Felicity ratios ≪ 1.00. However, there is a first indication, that Felicity ratios of fibre breakage related signals are typically larger than those of matrix cracking / interfacial failure related signals. This is in accordance with observations on macroscopic specimens [17].

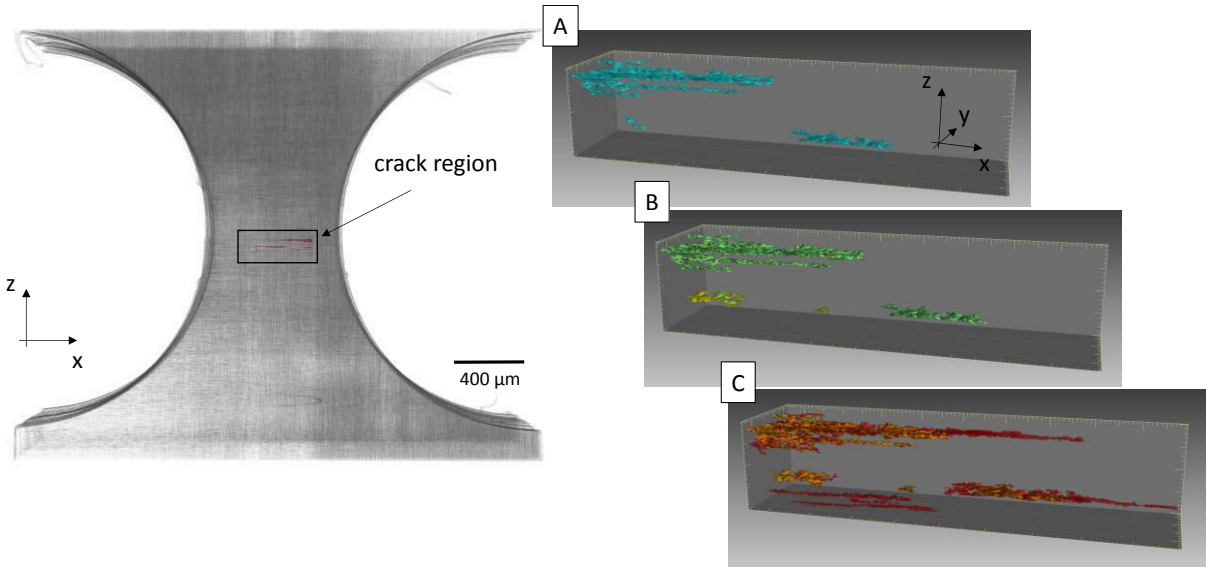

Figure 5. Visualization of inter-fibre crack and volumetric evaluation at three load levels (A-C) as noted in Figure 6.

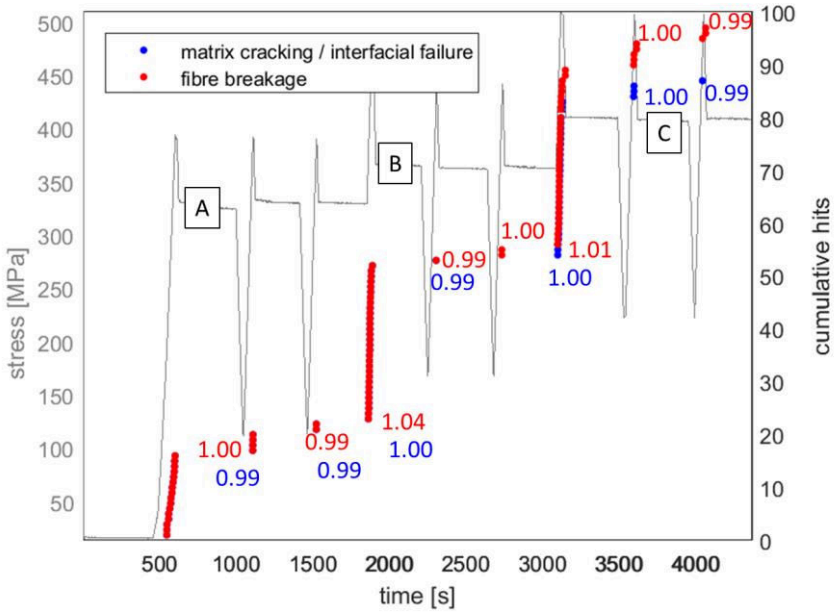

Figure 6. Example of layup [0 90_3 0] including Felicity Ratios evaluated for fibre breakage signals (red) and matrix cracking / interfacial failure related signals (blue).

3.2. Layup [±45 0 ±45]

As second case study, a ±45° dominated stacking sequence was investigated. In the evaluation of acoustic emission signals, two cycles result in Felicity ratios significantly lower than unity (i.e. FR = 0.85 and FR = 0.84). Until reaching a load level of 57% ultimate tensile strength, in SRCT the only significant damaged region is observed close to the notch positions. As seen in the SRCT slice example for load level A in Figure 7, part of this damage is already present in the beginning of the experiment (centre break, bright zone on right). Accordingly, it is likely, that this damage is a residue of the drilling process used to introduce the notches. At increased load levels (example at load level B) the number of cracks appears to grow. However, in all cases inspected, indications of the presence of these cracks is already found in the first (unloaded) SRCT scan. With applied load, the cracks are seen much better than in the unloaded case due to crack opening, resulting in the appearance of crack growth. However, the potential occurrence of additional damage growth in this area cannot be excluded. This is likely causing the numerous acoustic emission signals recorded in the experiment. Unfortunately, with no other evidence of crack growth from SRCT inspection, this does not allow a dedicated interpretation of the recorded Felicity ratios for this stacking sequence.

3.3. Layup [90 0_3 90]

As third case, a cross-ply stacking sequence with predominant fibre orientation in 0° was tested. Other than the test case of Section 3.1, this apparently results in less acoustic emission activity as seen in Figure 8. However, the Felicity ratios for this case are also consistently > 0.99, resulting in the same difficulty of interpretation of early onset acoustic emission signals. Similar to the previous cases, fibre breakage related signals apparently tend to result in slightly higher Felicity ratio values. In SRCT scans, we observed the occurrence of multiple fibre breaks. In the example shown in Figure 8, fibre breaks are visible at load level B located in

close proximity to a high-density inclusion (probably a dust particle introduced during specimen manufacture). Apart from that, no matrix cracks or delamination are visible in the SRCT scans.

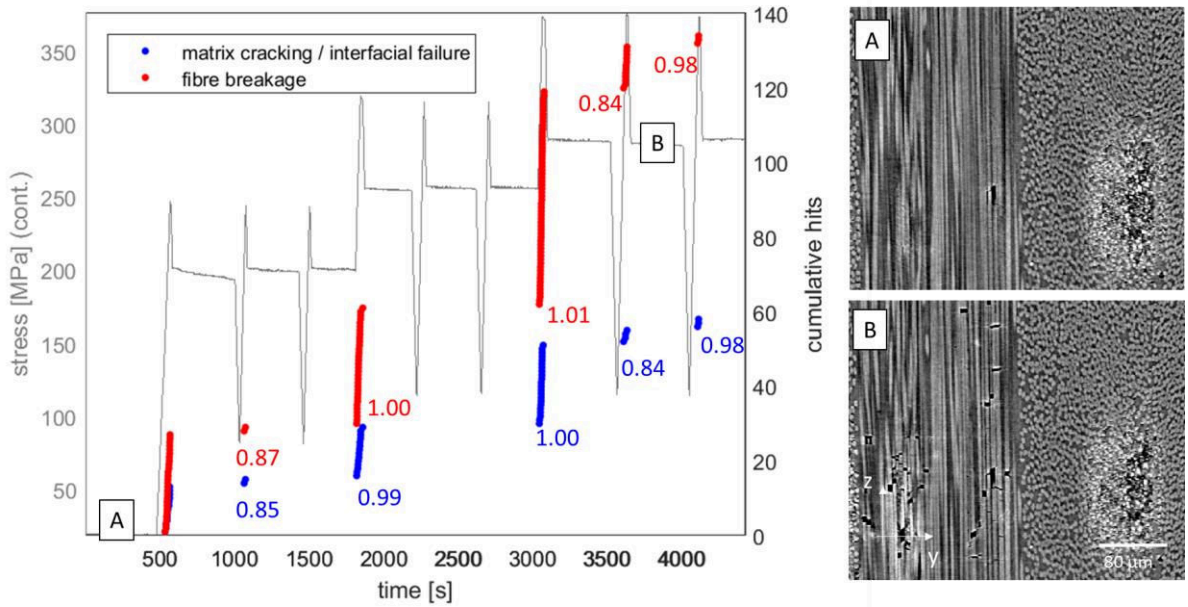

Figure 7. Example of layup [±45 0 ±45] including Felicity Ratios evaluated for fibre breakage signals (red) and matrix cracking / interfacial failure related signals (blue) and SRCT slices at two load levels (A-B).

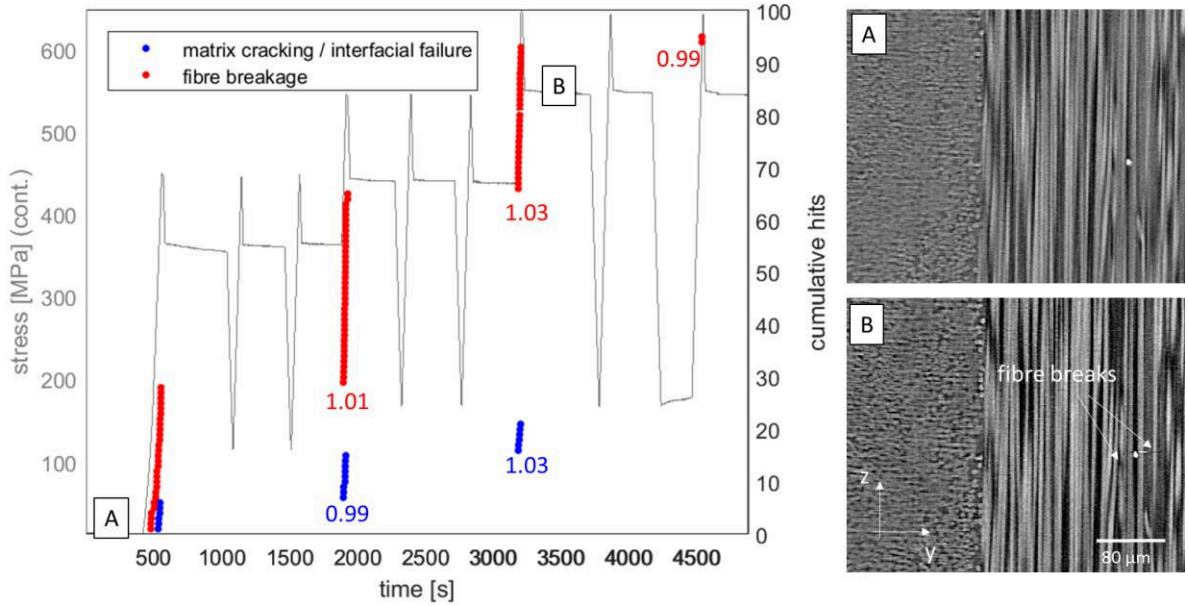

Figure 8. Example of layup [90 0_3 90] including Felicity Ratios evaluated for fibre breakage signals (red) and matrix cracking / interfacial failure related signals (blue) and SRCT slices at two load levels (A-B).

4. Conclusion

The combination of high-resolution SRCT and acoustic emission measurements has been successfully carried out during step-wise cyclic loading of fibre-reinforced materials. The overall experimental approach appears promising to reveal the origin of the Felicity effect in fibre-reinforced materials. However, in the present test campaign the vast majority of cases results in Felicity ratios ~ 1.0. Based on the tensile load and the layup used in these experiments, the fracture surfaces observed in SRCT are mode I dominated. No fracture surfaces were generated that are expected to undergo high tribological load during load/unload cycles. The only cases with Felicity ratios significantly below zero were the [±45 0 ±45] samples. Based on this layup, the expectation is a delamination damage growth between plies, resulting in mixed mode loading. However, the SRCT observation do not indicate such delamination growth in the experiments. Accordingly, the present data basis does not allow a final judgement on the true origin of the Felicity effect. However, a general trend of fibre breakage Felicity ratios being larger than for matrix cracking and interfacial failure related signals has been observed. This potentially indicates a difference in the origin of signal onset in these failure modes. Accordingly, future test campaigns should take into account different load concepts and layups to force the occurrence of shear loaded fracture surfaces. This might result in a higher number of test cases with low Felicity ratios.

Acknowledgments

The authors would like to acknowledge the European Synchrotron Radiation Facility for provision of synchrotron radiation facilities and would like to thank Dr. Lukas Helfen and Ms. Elodie Boller for assistance in using beamline ID19. The authors also gratefully acknowledge the µ-VIS X-Ray Imaging Centre at the University of Southampton for provision of tomographic imaging facilities, supported by EPSRC grant EP-H01506X.

References:

[1] T. J. Fowler, “Acoustic Emission Testing of Fiber Reinforced Plastics,” Proc. Pap. J. Tech. Counc. ASCE, vol. 105(TC2), pp. 281–289, 1977.
[2] J. Kaiser, “Untersuchungen über das Auftreten von Geräuschen beim Zugversuch,” Dissertation, Technische Hochschule München, 1950.
[3] J. Awerbuch, M. R. Gorman, and M. Madhukar, “Monitoring Acoustic Emission During Quasi-static Laoding-Unloading Cycles of Filament-wound Graphic-Epoxy Laminate Coupons,” Mater. Eval., vol. 43, no. 6, pp. 754–764, 1985.
[4] K. S. Downs and M. A. Hamstad, “Acoustic Emission from Depressurization to Detect/Evaluate Significance of Impact Damage to Graphite/Epoxy Pressure Vessels,” J. Compos. Mater., vol. 32, no. 3, pp. 258–307, Feb. 1998.
[5] W. Haselbach and B. Lauke, “Acoustic emission of debonding between fibre and matrix to evaluate local adhesion,” Compos. Sci. Technol., vol. 63, no. 15, pp. 2155–2162, Nov. 2003.
[6] M. R. Gorman, “Acoustic Emission in 2-D Carbon-Carbon Coupons in Tension,” J. Compos. Mater., vol. 25, no. 6, pp. 703–714, Jun. 1991.
[7] K. Ono, “Structural integrity evaluation using acoustic emission techniques,” J Acoust. Emiss., vol. 25, pp. 1–20, 2007.
[8] K. Ono and A. Gallego, “Research and Applications of AE on Advanced Composites,” J Acoust. Emiss., vol. 30, pp. 180–229, 2012.
[9] M. A. Hamstad, “A review: Acoustic emission, a tool for composite-materials studies,” Exp. Mech., vol. 26, no. 1, pp. 7–13, 1986.
[10] M. A. Hamstad, “Thirty years of advances and some remaining challenges in the

application of acoustic emission to composite materials," in Acoustic Emission Beyond the Millennium, S. Y. T. Kishi, M. Ohtsu, Ed. Amsterdam: Elsevier Science, 2000, pp. 77–91.

[11] P. Wright, X. Fu, I. Sinclair, and S. M. Spearing, "Ultra High Resolution Computed Tomography of Damage in Notched Carbon Fiber--Epoxy Composites," J. Compos. Mater., vol. 42, no. 19, pp. 1993–2002, Oct. 2008.

[12] A. E. Scott, M. Mavrogordato, P. Wright, I. Sinclair, and S. M. Spearing, "In situ fibre fracture measurement in carbon-epoxy laminates using high resolution computed tomography," Compos. Sci. Technol., vol. 71, no. 12, pp. 1471–1477, Aug. 2011.

[13] S. C. Garcea, M. N. Mavrogordato, A. E. Scott, I. Sinclair, and S. M. Spearing, "Fatigue micromechanism characterisation in carbon fibre reinforced polymers using synchrotron radiation computed tomography," Compos. Sci. Technol., vol. 99, pp. 23–30, Jul. 2014.

[14] S. C. Garcea, I. Sinclair, and S. M. Spearing, "Fibre failure assessment in carbon fibre reinforced polymers under fatigue loading by synchrotron X-ray computed tomography," Compos. Sci. Technol., vol. 133, pp. 157–164, Sep. 2016.

[15] P. Wright, A. Moffat, I. Sinclair, and S. M. Spearing, "High resolution tomographic imaging and modelling of notch tip damage in a laminated composite," Compos. Sci. Technol., vol. 70, no. 10, pp. 1444–1452, 2010.

[16] H. Akaike, "Markovian representation of stochastic process and its application to the analysis of autoregressive moving average processes," Ann. Inst. Stat. Math., vol. 26, pp. 363–387, 1974.

[17] M. G. R. Sause, In Situ Monitoring of Fiber-Reinforced Composites, vol. 242. Cham: Springer International Publishing, 2016.

[18] M. G. R. Sause, A. Gribov, A. R. Unwin, and S. Horn, "Pattern recognition approach to identify natural clusters of acoustic emission signals," Pattern Recognit. Lett., vol. 33, no. 1, pp. 17–23, Jan. 2012.

[19] P. Potstada, S. Rosini, M. Mavrogordato, I. Sinclair, M. Spearing, and M. G. R. Sause, "Cross-validation of single filament failure by acoustic emission and high-resolution synchrotron computed tomography," in ECCM18 - 18th European Conference on Composite Materials, 2018, pp. 1–8.

[20] M. G. R. Sause, T. Müller, A. Horoschenkoff, and S. Horn, "Quantification of failure mechanisms in mode-I loading of fiber reinforced plastics utilizing acoustic emission analysis," Compos. Sci. Technol., vol. 72, no. 2, pp. 167–174, Jan. 2012.

[21] M. G. R. Sause and S. Richler, "Finite Element Modelling of Cracks as Acoustic Emission Sources," J. Nondestruct. Eval., vol. 34, no. 1, p. 4, Mar. 2015.

[22] K. S. Downs and M. A. Hamstad, "Correlation of Acoustic Emission Felicity Ratios and Hold-Based Rate Moments with Burst Strngths of Spehrical Graphite/Epoxy Pressure Vessels," J. Acoust. Emiss., vol. 13, no. 3/4, pp. 45–56, 1995.

[23] M. G. R. Sause, S. Schmitt, and S. Kalafat, "Failure load prediction for fiber-reinforced composites based on acoustic emission," Compos. Sci. Technol., vol. 164, pp. 24–33, Aug. 2018.